In-situ investigation of the evolution of annealing twins in high purity aluminium

He, Qiongyao; Huang, Tianlin; Shuai, Linfei; Zhang, Yubin; Wu, Guilin; Huang, Xiaoxu; Juul Jensen, Dorte

Published in:
Scripta Materialia

Link to article, DOI:
10.1016/j.scriptamat.2018.04.034

Publication date:
2018

Document Version
Publisher's PDF, also known as Version of record

Scripta Materialia 153 (2018) 68–72

Contents lists available at ScienceDirect

Scripta Materialia

journal homepage: www.elsevier.com/locate/scriptamat

Regular article

In-situ investigation of the evolution of annealing twins in high purity aluminium

Qiongyao He [a], Tianlin Huang [a,c,*], Linfei Shuai [a], Yubin Zhang [b], Guilin Wu [a,**], Xiaoxu Huang [a,b], Dorte Juul Jensen [a,b]

[a] International Joint Laboratory for Light Alloys (Ministry of Education), College of Materials Science and Engineering, Chongqing University, Chongqing 400044, China
[b] Department of Mechanical Engineering, Technical University of Denmark, DK-2800 Lyngby, Denmark
[c] Electron Microscopy Center of Chongqing University, Chongqing University, Chongqing 400044, China

ARTICLE INFO

Article history:
Received 22 February 2018
Received in revised form 20 April 2018
Accepted 21 April 2018
Available online xxxx

Keywords:
Aluminium
Annealing twins
In-situ annealing
EBSD

ABSTRACT

With focus on annealing twins, the microstructural evolution of cold rolled high purity aluminium was characterized in-situ during annealing using the electron backscatter diffraction technique. It was found that annealing twins developed during recrystallization. Many but not all of the twins were gradually removed during grain growth. The grain boundary energies of all the boundaries in a network associated with the twins are estimated and reasons why most twins disappear while a few remain are discussed.

Annealing twins are frequently observed in face center cubic (FCC) metals with low or medium stacking fault energies (SFEs), i.e. Cu [1], Ag [2], and Ni [3–6]. Formation of annealing twins in these metals results in grains with a variety of orientations that can eventually grow and thus significantly affect the microstructures and textures [7]. Annealing twins in these metals have also been considered to improve properties such as corrosion [8,9] and fatigue resistance [10] due to the low energy of twin boundaries, which is the basis for grain boundary engineering [11].

Annealing twins in Al and Al alloys with high SFEs, however, are much rarer; and in fully recrystallized Al as well as in Al annealed to grain growth, hardly any twins are observed. This is particularly interesting as several authors have observed many annealing twins in the early stages of recrystallization. Key examples of this include: Berger et al. [12,13] observed a twin-relationship between the deformed and recrystallized nuclei during in-situ annealing of Al by high-voltage electron microscopy; Xu et al. [14] characterized nuclei forming during annealing beneath a microhardness tip in an Al crystal and detected nuclei with twin relationships to the deformed matrix; Humphreys and Ferry et al. [15] found formation of annealing twins related to particle-stimulated nucleation in an Al-Si alloy. It is thus a puzzle what happens with the annealing twins formed early in the recrystallization process, how and why do they disappear. An investigation of this is the purpose of the present work.

Recently, in a preliminary investigation, Wu et al. [16] reported removal of annealing twins in Al-0.3%Mg during annealing. However, the evolution of twins and the nearby grain boundary regions were not investigated in their work. In the present study, the microstructural evolution of a cold rolled high purity Al during annealing was followed by electron backscatter diffraction (EBSD) using an in-situ heating stage in a scanning electron microscope (SEM), which allows direct observation of the evolution of annealing twins at the sample surface. It is reported that annealing twins develop more frequently at the surface than in the bulk [15]. This is considered an advantage for the present investigation.

The starting material was 99.996% purity Al cold rolled to a reduction of 25% in thickness. A sample 5 mm long (along rolling direction, RD), 3 mm thick (along normal direction, ND) and 1 mm wide (along transverse direction, TD) was cut from the rolled sheet. The RD-ND section of the sample was ground, followed by electropolishing. It was observed that the microstructure of the deformed sample is composed of very large original grains (average size of ~1 mm) containing many deformation-induced low angle boundaries (see Fig. 1a). In-situ heating was performed with a home-made heating stage in a FEI Nova 400 thermal field emission gun SEM. The sample was annealed by two heating units at the two ends of sample, and the temperature was measured by a thermocouple directly touching the backside of the sample opposite to the EBSD detector. The annealing schedule to the maximum

* Correspondence to: T. Huang, International Joint Laboratory for Light Alloys (Ministry of Education), College of Materials Science and Engineering, Chongqing University, Chongqing 400044, China.
** Corresponding author.
E-mail addresses: huangtl@cqu.edu.cn, (T. Huang), wugl@cqu.edu.cn (G. Wu).

https://doi.org/10.1016/j.scriptamat.2018.04.034

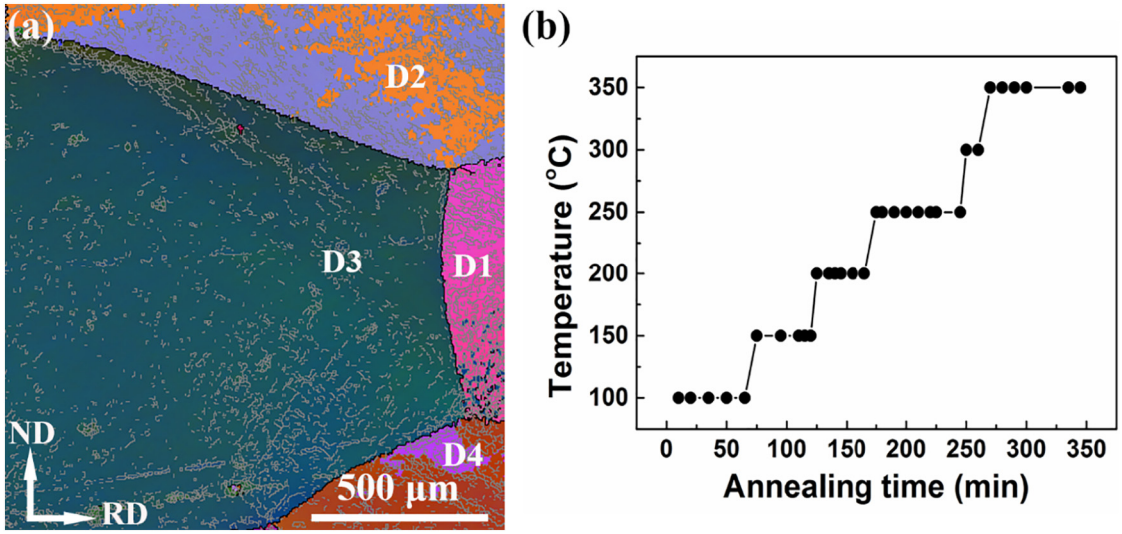

Fig. 1. (a) EBSD map of the deformed microstructure. The gray, black, and white lines in the map show boundaries with misorientation above 2°, 15° and twin boundaries, respectively. (b) The annealing sequence.

annealing temperature of 350 °C and a total annealing time of approximately 6 h is illustrated in Fig. 1b. The microstructure of the sample at each annealing step was characterized by EBSD using a step size of 5 μm to compromise between a fast acquisition time (~5 min) and a large sampling area (~1 mm × 0.8 mm). Twin boundaries were identified having a maximum deviation of 1.5° from the Σ3, 60°/⟨111⟩ misorientation relationship, and are shown as white lines in Figs. 2–4.

Fig. 2a shows an EBSD map of the sample after annealing at 150 °C. Compared to the map in the deformed state, the observed area in the annealed state is shifted about 800 μm to reveal the entire grain D1. Both annealing twins and recrystallizing grains are found to form within D1, whereas the grains D2-D4 have not yet started to recrystallize. Within D1, two twin boundaries named TB1 and TB2 with lengths of tens to hundreds of micrometers, respectively, are observed separating recrystallizing grains. Two "regular twins" labeled T3 and T4 with approximately parallel straight boundary traces have developed within the recrystallized grain R5, with one end of the twins attached to the grain boundary of R5.

Several mechanisms may have led to the formation of these twins and twin boundaries: as can be seen from Fig. 2b, the two grains, R1 and R2, are twin orientation-related; and both grains have a ⟨111⟩ type misorientation to the deformed matrix. A similar orientation relationship is observed between the two grains R3 and R4 (separated by TB1) and the deformed matrix. In previous works [17,18], nuclei misoriented to the deformed matrix by a rotation around a common ⟨111⟩ axis have been reported, and in other works [12,13,19], it is observed that when a nucleus is formed, it may continue to grow by twinning. Both these observations may well explain the presence of TB1 and TB2 in our work. However, as each of the recrystallized grain separated by TB1 and TB2 shares a common ⟨111⟩ twinning plane with the deformed matrix, it is not possible to conclude which grain developed first.

The regular twins, T3 and T4, have an orientation within the spread of the deformed grains, D1 and D2, respectively (see Fig. 2c), and are contained within the recrystallized grain R5. There are also near twin relationships between R5 and both T3 and T4 as well as between R5 and both D1 and D2 (50–52°⟨111⟩). Because of the similarity in orientation between the twin and the deformed grain, it is very likely that the twins nucleated from the deformed grains and R5 formed by growth twinning.

As the main aim of the present work is to follow the evolution of twins as a function of recrystallization and grain growth, it is an advantage that we in the investigated area have twin boundaries separating recrystallized grain, i.e. TB1 and TB2 as well as boundaries surrounding "regular twins" i.e. T3 and T4.

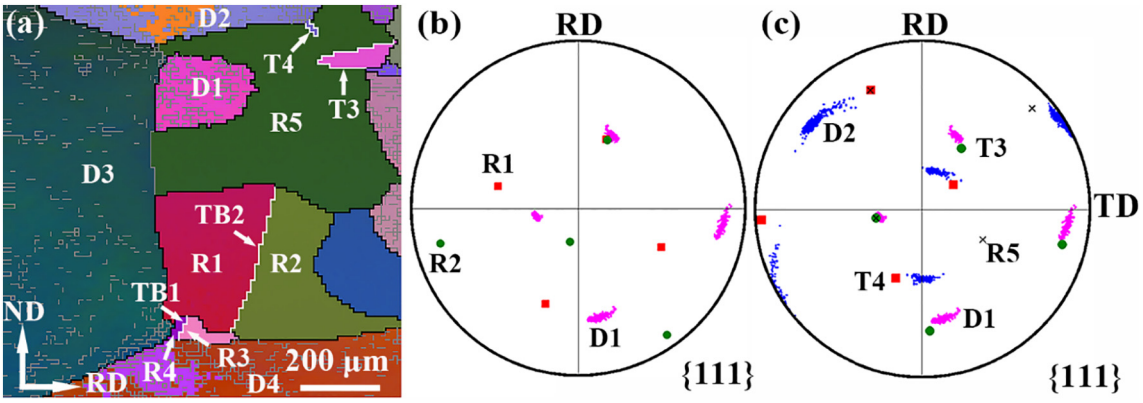

Fig. 2. (a) EBSD map of the microstructure after annealing at 150 °C for 40 min. The gray, black and white lines in the map indicate grain boundaries above 2°, 15° and twin boundaries, respectively. (b) {111} pole figure of the deformed grain D1 plus the grains R1 and R2. Pink dots represent the orientations of the deformed grain D1; red squares and green circles represent the grain R1 and R2, respectively. (c) {111} pole figure of the deformed grains D1, D2, the recrystallizing grain R5 and the annealing twins T3 and T4. Pink and blue dots represent the orientations of the deformed grain D1 and D2, respectively; while green circles, red squares and black crosses represent the T3, T4 and R5, respectively. (For interpretation of the references to color in this figure legend, the reader is referred to the web version of this article.)

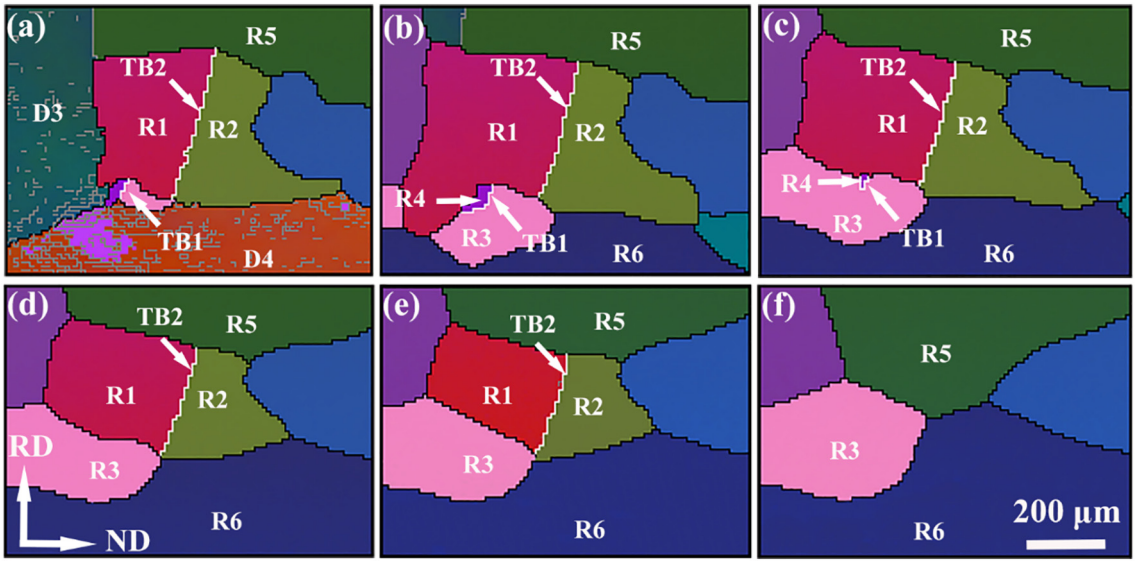

Fig. 3. EBSD maps showing the microstructural evolution of twin boundaries TB1 and TB2 after annealing at (a) 200 °C for 5 min; (b) 250 °C for 70 min; (c) 300 °C for 5 min; (d) 350 °C for 5 min; (e) 350 °C for 15 min and (f) 350 °C for 25 min.

Fig. 3 illustrates the microstructural evolution of the twin boundaries TB1 and TB2 upon further annealing. It should be noted that after the annealing step of 250 °C for 70 min (Fig. 3b), the local area is completely recrystallized. As Fig. 3 reveals, both twin boundaries TB1 and TB2 are essentially stationary during the annealing, which is as expected. They are however both removed because either one or both of the recrystallized grains separated by those stationary twin boundaries are 'consumed' by neighboring grains during grain growth.

Thereby the total boundary energy (i.e. the energy per unit length of both the grain and the twin boundary) within the area is reduced. The reduction of energy per unit length, ΔE, can be estimated using the following equation [20]:

$$\Delta E = \sigma_{GB}\Delta l_{GB} + \sigma_{TB}\Delta l_{TB} \quad (1)$$

where the energy of the grain boundary, σ_{GB}, and the twin boundary, σ_{TB}, of pure Al are 0.324 J/m^2 and 0.075 J/m^2 [20], respectively; and Δl_{GB} and Δl_{TB} are the change in lengths of the grain boundary and twin boundary, respectively. It is found that the reduction in boundary energy from Fig. 3b to f is ~1.01 kJ/μm. Energy reduction can thus explain why these annealing twin boundaries are removed. In this respect, it is important to note that in Al the twin boundary energy is ~24% of the high angle grain boundary energy [20], whereas in Cu it is only ~4% [20]. This may explain why it is energetically favorable to keep many twins in Cu, while they are removed in Al during annealing.

Fig. 4 shows the microstructural evolution of the area containing the two twins T3 and T4. The local area near T3 and T4 is completely recrystallized after annealing at 250 °C for 25 min (Fig. 4b). D2 has been replaced by several recrystallized grains (R8–R10). But at this stage none of these grains seems to affect the twins T3 and T4. It is interesting to note that T3 is eliminated during the annealing while T4 actually grows to become larger. To the authors' knowledge, such a continuous increase in length has not before been reported for annealing twins in Al during grain growth.

By relating to the fix points marked by red crosses in Fig. 4, it is clear that both the grain boundary GB1 and GB2, to which the twins are attached, as well as the tips of the twins migrate significantly during the annealing. The average migration velocities were measured from the

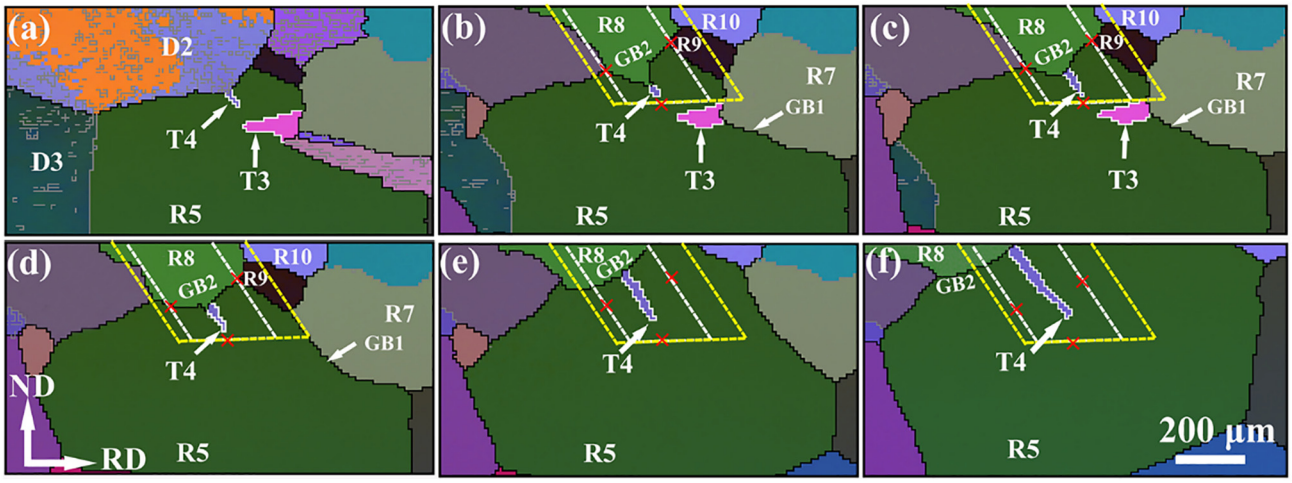

Fig. 4. EBSD maps of the microstructural evolution of the twins T3 and T4 after annealing at (a) 200 °C for 5 min; (b) 250 °C for 25 min; (c) 250 °C for 70 min; (d) 300 °C for 5 min; (e) 350 °C for 15 min and (f) 350 °C for 80 min. The red crosses mark the exactly same positions in figs. b–f. The white and yellow parallelograms are used to calculate the total localized boundary energy. (For interpretation of the references to color in this figure legend, the reader is referred to the web version of this article.)

Table 1
Average boundary migration velocities of GB1, GB2 and the tips of T3, T4 at different annealing temperatures and the corresponding activation energies.

	Average boundary migration velocity at different temperature (μm/min)			Activation energy (kJ/mol)	
	250 °C	300 °C	350 °C	250 °C–300 °C	300 °C–350 °C
Grain boundary GB1	0.39 ± 0.06	3.44 ± 0.43	–	108.49	–
Twin tip of T3	0.81 ± 0.26	6.47 ± 0.52	–	103.54	–
Grain boundary GB2	0.92 ± 0.08	1.83 ± 0.48	2.04 ± 0.15	34.27	6.45
Twin tip of T4	0.46 ± 0.12	0.20 ± 0.42	0.53 ± 0.13	−41.50	57.85

Table 2
Total energy change at the various annealing steps in Fig. 4b–f. The region I and II refer to the white and yellow parallelograms shown in Fig. 4, respectively.

	Annealing step			
	Fig. 4b–c	Fig. 4c–d	Fig. 4d–e	Fig. 4e–f
Total boundary energy change in Region I, J/μm	−12.58	−3.31	7.07	−6.19
Total boundary energy change in Region II, J/μm	−19.38	−29.23	−74.62	−3.60

series of EBSD maps obtained at a given annealing temperature and the results are reported in Table 1. As velocities are measured at different temperatures, activation energies may also be calculated using the equation [21]:

$$Q = R\left(\frac{1}{T1} - \frac{1}{T2}\right) \ln\frac{v_2}{v_1} \quad (2)$$

where Q is the activation energy, R is the gas constant, T1 and T2 are the absolutely temperatures, and v_1, v_2 are the migration velocities at T1 and T2, respectively. The data show a large variation in migration velocity and in activation energy. Some of the calculated activation energies are within the range of 84–142 kJ/mol generally reported for Al in literature [20], but also smaller values and even a negative activation energy is observed. This is not in accord with standard conception. However, synchrotron x-ray measurements have shown that the activation energies for migration of individual boundaries, have a very wide distribution with values down to zero [21], and numerical simulations have suggested that dependent on the boundary misorientation and plane, negative, zero or positive activation energies may be expected [22,23]. Other parameters of importance for the boundary migration velocity and thus the activation energy are the local boundary curvature and small impurities and particles, which may pin the boundary. A large local curvature of GB2 at T4 is for example seen in Fig. 4 which temporally may speed up the migration of GB2. In agreement with the present and earlier results [21,24], it is thus clear that the migration of individual grain boundaries as well as twin boundaries may vary significantly depending on a boundary itself and the microstructure into which it moves.

In spite of the local variation, there are common trends in the data shown in Table 1: the tip of T3 migrates faster than GB1, whereas the tip of T4 migrates slower than GB2. As a consequence, T3 is finally eliminated and T4 extends in length. The elimination of T3 follows the pattern discussed above, while T4 is in contradiction.

To understand why T4 is surviving and even growing in size, the total boundary energies in selected local regions around T4 were calculated. Both a narrow region (indicated by the white dotted lines in Fig. 4) around T4 and a wider region (indicated by the yellow dotted lines in Fig. 4) including the neighboring triple junctions are selected. The results are given in Table 2. When only the small region is considered, it is found that the energy reduction upon annealing is marginal and it appears that the energy is actually increasing in one of the annealing steps. However, when the wider region is considered, the energy is reduced in all annealing steps. As the grain boundary network is in 3D and we here only observe that on the inspected 2D surface, it is clear that this calculation does not give the complete description. However, because of the connectivity between grain boundaries and because the boundaries cannot be assumed to migrate by single atom jumps but rather by concerted actions between many atoms [25], it is reasonable that energy balances have to be considered over a larger, not very local region.

In summary, the evolution of annealing twins in 25% cold rolled high purity Al has been characterized in-situ by EBSD. The results show that many annealing twins develop during early stages of recrystallization. Most of annealing twins disappear during grain growth and the migration velocities of both incoherent twin boundaries and individual grain boundaries vary a lot giving rise to a wide distribution of activation energies. One annealing twin formed on a boundary with a large curvature is observed to grow to a large size, resulting in a local boundary energy increase associated with the growing twin. However, it is found that the total boundary energies are reduced when all the boundaries in a not too small region around the twin (including neighboring grain boundaries and triple junction) are included in the calculation. For all the observed annealing twins, it is thus concluded that their evolution is strongly affected by the migration of the grain boundaries adjacent to the twin boundaries and is governed by a reduction in energy of the total boundary network.

Acknowledgments

This project was financially supported by the National Natural Science Foundation of China (NSFC, funding Nos. 51471039, 51327805 and 51421001). QYH thanks the Graduate Student Research Innovation Project of Chongqing University (No. CYB14007). DJJ thanks for the support of the 111 Project (B16007) by the Ministry of Education and the State Administration of Foreign Experts Affairs of China.

References

[1] D. Field, L. Bradford, M. Nowell, T. Lillo, Acta Mater. 55 (2007) 4233–4241.
[2] T.H. Chuang, H.C. Wang, C.H. Tsai, C.C. Chang, C.H. Chuang, J.D. Lee, H.H. Tsai, Scr. Mater. 67 (2012) 605–608.
[3] B. Lin, Y. Jin, C.M. Hefferan, S.F. Li, J. Lind, R.M. Suter, M. Bernacki, N. Bozzolo, A.D. Rollett, G.S. Rohrer, Acta Mater. 99 (2015) 63–68.
[4] J.L. Bair, S.L. Hatch, D.P. Field, Scr. Mater. 81 (2014) 52–55.
[5] V. Randle, P.R. Rios, Y. Hu, Scr. Mater. 58 (2008) 130–133.
[6] Y.B. Zhang, A. Godfrey, W. Liu, Q. Liu, Mater. Sci. Technol. 26 (2010) 197–202.
[7] K.H. Song, Y.B. Chun, S.K. Hwang, Mater. Sci. Eng. A 454–455 (2007) 629–636.
[8] C.M. Barr, G.A. Vetterick, K.A. Unocic, K. Hattar, X.M. Bai, M.L. Taheri, Acta Mater. 67 (2014) 145–155.
[9] C. Hu, S. Xia, H. Li, T. Liu, B. Zhou, W. Chen, N. Wang, Corros. Sci. 53 (2011) 1880–1886.
[10] B.B. Rath, M.A. Imam, C.S. Pande, Mater. Phys. Mech. 1 (2000) 61–66.
[11] T. Watanabe, Res. Mech. 11 (1984) 47–84.
[12] A. Berger, P.J. Wilbrandt, F. Ernst, U. Klement, P. Haasen, Prog. Mater. Sci. 32 (1988) 1–95.
[13] A. Berger, P.J. Wilbrandt, P. Haasen, Acta Metall. 31 (1983) 1433–1443.
[14] C. Xu, Y. Zhang, A. Godfrey, G. Wu, W. Liu, J.Z. Tischler, Q. Liu, D. Juul Jensen, Sci. Rep. 42508 (2017) 1–7.

[15] F.J. Humphreys, M. Ferry, Scr. Mater. 35 (1996) 99–105.
[16] G.L. Wu, H.S. Ubhi, M. Petrenec, D. Juul Jensen, IOP Conf. Series Mater. Sci. Eng. 89 (2015), 012051. .
[17] G.L. Wu, D. Juul Jensen, Acta Mater. 55 (2007) 4955–4964.
[18] T.J. Sabin, G. Winther, D. Juul Jensen, Acta Mater. 51 (2003) 3999–4011.
[19] H. Paul, J.H. Driver, C. Maurice, A. Piatkowski, Acta Mater. 55 (2007) 833–847.
[20] F.J. Humphreys, M. Hatherly, Recrystallization and Related Annealing Phenomena, 2nd ed. Pergamon Press, Oxford, 2004.
[21] S.O. Poulsen, E.M. Lauridsen, A. Lyckegaard, J. Oddershede, C. Gundlach, C. Curfs, D. Juul Jensen, Scr. Mater. 64 (2011) 1003–1006.
[22] E.A. Holm, S.M. Foiles, Science 328 (2010) 1138–1141.
[23] D.L. Olmsted, E.A. Holm, S.M. Foiles, Acta Mater. 57 (2009) 3704–3713.
[24] G.L. Wu, D. Juul Jensen, Philos. Mag. 92 (2012) 3381–3391.
[25] A.P. Sutton, R.W. Balluffi, Interfaces in Crystalline Materials, Clarendon Press, Oxford, 1995.